



## Kinetics and speciation of paraoxon hydrolysis by zinc(II)–azamacrocyclic catalysts



Daniel J. Kennedy<sup>a,b</sup>, Brian P. Mayer<sup>a,b</sup>, Sarah E. Baker<sup>b</sup>, Carlos A. Valdez<sup>a,b,\*</sup>

<sup>a</sup> Forensic Science Center, Lawrence Livermore National Laboratory, 7000 East Avenue, L-091, Livermore, CA 94550, USA

<sup>b</sup> Physical and Life Sciences Directorate, Lawrence Livermore National Laboratory, 7000 East Avenue, Livermore, CA 94550, USA

### ARTICLE INFO

#### Article history:

Received 8 June 2015

Received in revised form 14 July 2015

Accepted 22 July 2015

Available online 3 August 2015

#### Keywords:

Pesticides

Organophosphorus

Hydrolysis

Catalysis

Zinc

Phosphotriester

### ABSTRACT

Four Zn<sup>2+</sup>–azamacrocyclic complexes were investigated for their ability to catalyze the hydrolysis of the toxic organophosphate (OP) pesticide diethyl paraoxon. Of the four complexes studied, Zn<sup>2+</sup>–1,5,9-triazacyclododecane (Zn<sup>2+</sup>–[12]aneN<sub>3</sub>) was found to be the most effective catalyst with a pseudo-first order reaction rate of  $k = 6.08 \pm 0.23 \times 10^{-4} \text{ min}^{-1}$ . Using <sup>31</sup>P nuclear magnetic resonance (NMR) spectroscopy, the two products diethyl phosphate (DEP) and ethyl (4-nitrophenyl) phosphate (E4NPP) were identified for both catalyzed and background hydrolysis of paraoxon. Reaction rate and selectivity for formation of the non-toxic DEP were observed to correlate with catalyst pK<sub>a</sub>. The rate of formation of toxic E4NPP, however, was independent of both the presence and nature of the catalyst. The potential roles of buffer concentration and product inhibition were also investigated. Background hydrolysis at elevated reaction temperatures (50 °C) displayed no preference for DEP over that of E4NPP despite substantial differences between the characteristics (i.e., pK<sub>a</sub> values) of the two leaving groups (ethoxide vs. 4-nitrophenoxide anions). As with previous observations of these types of metal-catalyzed hydrolyses, we invoke the formation of a trigonal bipyramidal-like transition state involving a Zn-coordinated phosphate bond, with the leaving group at the apical position and the incoming HO<sup>−</sup> anion approaching from the opposite end. Kinetic rates for catalytic hydrolysis display an overwhelming propensity for DEP formation, and suggest the importance of steric restrictions on transition state structure, namely a concerted arrangement of the azamacrocyclic in opposition to the bulky 4-nitrophenoxy group.

© 2015 Elsevier B.V. All rights reserved.

## 1. Introduction

In spite of their usefulness as agricultural pest deterrents, organophosphorus (OP) pesticides are known to possess physical and chemical properties which cause detrimental environmental and physiological effects [1–3]. For example, many OPs have high boiling points and are relatively unreactive, making them potentially persistent environmental hazards [4,5]. From a physiological perspective, many are acutely toxic through their irreversible inhibition of cholinesterases. The most acutely toxic OP compounds, characterized by a high degree of reactivity and low chemical stability, have been developed and used as chemical warfare agents (CWAs) for military and terrorist activities (e.g. sarin, soman, and VX). These troubling properties reflect a critical need for

methodologies and technologies that are effective at neutralizing the physical and biological impact of many OP compounds.

Azamacrocyclic organometallic compounds are known for their ability to catalyze the degradation of a wide variety of carboxy- [6,7] and phosphorus-based [8–10] esters, making them potential candidates for the degradation of toxic OP compounds. 1,4,7-triazacyclononane ([9]aneN<sub>3</sub>), 1,5,9-triazacyclododecane ([12]aneN<sub>3</sub>), 1,4,7,10-tetraazacyclododecane ([12]aneN<sub>4</sub> or cyclen), and 1,4,8,11-tetraazacyclotetradecane ([14]aneN<sub>4</sub> or cyclam) (Chart 1A–D, respectively) are members of this class of cyclic compounds and are recognized as suitable ligands for a variety of metal ions including Zn<sup>2+</sup>, Co<sup>3+</sup>, Cu<sup>2+</sup>, Ni<sup>3+</sup>, and Fe<sup>3+</sup> [11–16]. In aqueous solutions, the metal center coordinates the ligand's nitrogen atoms and a water molecule which may exist as a catalytically active hydroxide ion at a suitable pH. The electronic properties of the macrocyclic ligand and the number of coordinating nitrogens directly influence the pK<sub>a</sub> [17]. For example, the coordinated water of the Zn<sup>2+</sup>–[12]aneN<sub>3</sub> complex exhibits one of the lowest known pK<sub>a</sub> values (pK<sub>a</sub> = 7.3 in water at 50 °C) within this class of compounds [18,19]. Thus, it is not surprising to find that even in

\* Corresponding author at: Forensic Science Center, Lawrence Livermore National Laboratory, 7000 East Avenue, L-091, Livermore, CA 94550, USA. Tel.: +1 925 423 1804; fax: +1 925 423 9014.

E-mail address: [valdez11@llnl.gov](mailto:valdez11@llnl.gov) (C.A. Valdez).

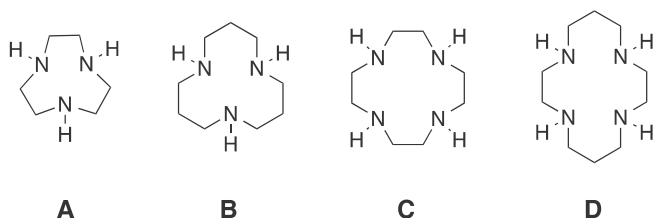


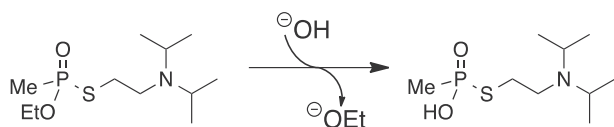
**Chart 1.** Structures of the nitrogen-containing ligands used for  $\text{Zn}^{2+}$  catalyst synthesis: (A) 1,4,7-triazacyclononane ([9]aneN<sub>3</sub>), (B) 1,5,9-triazacyclododecane ([12]aneN<sub>3</sub>), (C) 1,4,7,10-tetraazacyclododecane ([12]aneN<sub>4</sub> or cyclen), and (D) 1,4,8,11-tetraazacyclotetradecane ([14]aneN<sub>4</sub> or cyclam).

slightly basic solutions, complexes with low  $\text{pK}_a$  values (such as  $\text{Zn}^{2+}$ -[12]aneN<sub>3</sub>) overwhelmingly exist in their activated hydroxide ion forms (e.g. >94%  $\text{Zn}^{2+}$ -[12]aneN<sub>3</sub>-OH<sup>-</sup> vs. <6%  $\text{Zn}^{2+}$ -[12]aneN<sub>3</sub>-OH<sub>2</sub> at pH = 8.5 in water at 50 °C). This value is quite low compared to those exhibited by  $\text{Zn}^{2+}$ -cyclen ( $\text{pK}_a = 8.0$ ) [18,20] and  $\text{Zn}^{2+}$ -cyclam ( $\text{pK}_a = 9.8$ ) [20]. Under the same conditions,  $\text{Zn}^{2+}$ -cyclen and  $\text{Zn}^{2+}$ -cyclam have active fractions of 76.0% and 4.8%, respectively.

Though metal-azamacrocyclic complexes are potentially effective catalysts for neutralization of OP pesticides and CWAs, catalytic activity is not a sufficient criterion for determining ideal candidates for decontamination applications. The hydrolysis should not generate products that can bind the metal center (e.g. the thiolate generated from VX hydrolysis) and cause inactivation of the catalyst [21]. Product selectivity must be considered, as many degradation products display toxicities similar to those of the pesticides and CWAs themselves. For example (see Scheme 1), EA-2192 (*S*-[2-(diisopropylamino)ethyl] methylphosphonothioate), generated from the hydrolysis of the nerve agent VX (*O*-ethyl *S*-[2-(diisopropylamino)ethyl] methylphosphonothioate), is known to display similar toxicity to its parent compound [22]. Thus, an effective catalyst from a neutralization perspective should display selectivity towards the production of degradation products which are nontoxic in comparison to their parent compounds.

Lastly, within the realm of CWA decontamination, the applied technology needs to be selective only against the agents, leaving surfaces, expensive equipment, and contaminated areas as intact as possible. To date, effective decontamination technologies make use of excess amounts of highly corrosive and caustic solutions such as bleach and other basic formulations (pH > 11) [23–25]. Extensive efforts, including those described herein, are now being directed towards the development of affordable catalytic technologies for the large-scale defeat of these toxic substances.

In the present work, we assess a panel of four zinc(II)-azamacrocyclic complexes for effectiveness in the degradation of the OP pesticide paraoxon (*O,O*-diethyl *O*-(4-nitrophenyl) phosphate), the oxidase metabolite of the pesticide parathion (*O,O*-diethyl *O*-(4-nitrophenyl) phosphorothioate) (see Chart 2). The complexes were evaluated for their catalytic properties in AMPSO (*N*-(1,1-dimethyl-2-hydroxyethyl)-3-amino-2-hydroxypropanesulfonic acid) buffer (initial pH = 8.5) at 50 °C, and the extent of paraoxon degradation was followed using <sup>31</sup>P nuclear magnetic resonance



**Scheme 1.** General hydrolysis of the nerve agent VX (*O*-ethyl *S*-[2-(diisopropylamino)ethyl] methylphosphonothioate) resulting in a similarly toxic product, EA-2192 (*S*-[2-(diisopropylamino)ethyl] methylphosphonothioate).

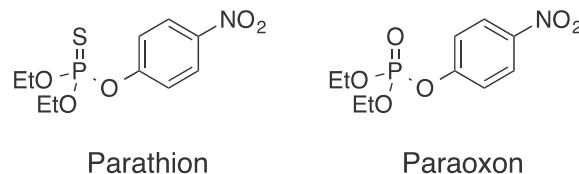
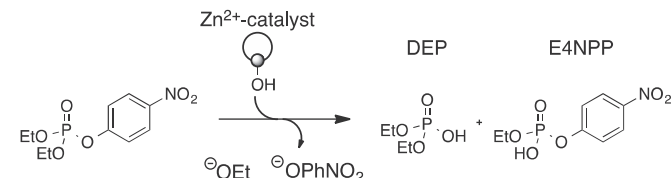


**Chart 2.** Structures of parathion (*O,O*-diethyl *O*-(4-nitrophenyl) phosphorothioate, left) and its oxidase metabolite, paraoxon (*O,O*-diethyl *O*-(4-nitrophenyl) phosphate, right).



**Scheme 2.** Paraoxon degradation products, diethyl phosphate (DEP, left) and ethyl (4-nitrophenyl) phosphate (E4NPP, right) by a general  $\text{Zn}^{2+}$ -catalyst.

(NMR). Timescales for complete degradation were on the order of days for solutions containing 10 mol% catalyst relative to the initial paraoxon concentration. Selectivity of the reaction products, nontoxic diethyl phosphate (DEP) and the potentially toxic ethyl (4-nitrophenyl) phosphate (E4NPP), was monitored as well (Scheme 2). For the most active catalyst,  $\text{Zn}^{2+}$ -[12]aneN<sub>3</sub>, we further investigated the effects of substrate concentration, buffer concentration, and product inhibition on overall catalytic activity.

## 2. Materials and methods

### 2.1. General

All reagents used were of analytical grade, purchased from commercial suppliers, and used as received. The cyclam ([14]aneN<sub>4</sub>) and [12]aneN<sub>3</sub> ligands were purchased from Alfa Aesar (Ward Hill, MA), [9]aneN<sub>3</sub> was purchased from TCI America (Portland, OR), and cyclen ([12]aneN<sub>4</sub>) was purchased from Strem Chemicals (Newburyport, MA). The syntheses of all catalysts employed in this study were carried out as previously reported [17]. Paraoxon, zinc perchlorate hexahydrate, and AMPSO were purchased from Aldrich Chemicals (St. Louis, MO). The different AMPSO buffers used (0.1, 0.25 and 0.5 M; pH 9.1 at 25 °C in water, 8.5 at 50 °C in water, 8.1 at 50 °C in a mixture consisting of 50% H<sub>2</sub>O, 37.5% D<sub>2</sub>O, and 12.5% CD<sub>3</sub>CN) were prepared using Milli-Q water and were refrigerated until use. Hexamethylphosphoramide (HMPA), a common internal chemical shift standard for <sup>31</sup>P NMR experiments, was purchased from Sigma Aldrich (St. Louis, MO). Deuterated acetonitrile (CD<sub>3</sub>CN) and water (D<sub>2</sub>O) were purchased from TCI America (Portland, OR). All pH values are expressed on an absolute scale in reference to water as the standard state solvent.

### 2.2. Sample preparation

Kinetics of paraoxon hydrolysis were monitored with <sup>31</sup>P NMR. The NMR samples were prepared in triplicate as follows: in a 5 mm NMR tube, 50  $\mu\text{L}$  of a 40 mM solution of HMPA in D<sub>2</sub>O was added to 200  $\mu\text{L}$  of the AMPSO buffer using a pipette. 100  $\mu\text{L}$  of the stock catalyst solution (5.45 mM in D<sub>2</sub>O) was added via pipette. 50  $\mu\text{L}$  of a 0.109 M solution of paraoxon in CD<sub>3</sub>CN was added to the solution and incubated at 50 °C in an oil bath. This yielded 13.6 mM paraoxon and 1.36 mM catalyst in a mixture consisting of 50% H<sub>2</sub>O, 37.5% D<sub>2</sub>O, and 12.5% CD<sub>3</sub>CN. In all cases, the initially colorless solutions eventually turned bright yellow, indicating the

generation of 4-nitrophenol (4-NP). Throughout the course of these reactions (at an initial pH of 8.1 and kept at 50 °C for a week), the HMPA remained unreactive, making it a suitable choice as an internal standard for both chemical shift and quantitation purposes.

### 2.3. NMR analysis

All experiments were conducted on a Bruker Avance III 600 MHz instrument equipped with a Bruker QNP 5 mm cryoprobe (Bruker Biospin, Billerica, MA) at  $30.0 \pm 0.1$  °C. The pulse sequences used were default experiments provided by the manufacturer. Ninety-degree pulse lengths of 18.2  $\mu$ s for  $^1\text{H}$  and 9.0  $\mu$ s for  $^{31}\text{P}$  were manually determined via nutation experiments.

As  $^{31}\text{P}$  spectra are straightforward to interpret with relatively few, well-resolved resonances, this nucleus was chosen to monitor paraoxon degradation. To allow proper quantitation for the kinetic experiments, measurements of the longitudinal relaxation time  $T_1$  were conducted for each  $^{31}\text{P}$  resonance. A traditional inversion recovery pulse sequence was used and the resulting data were fit to an exponential growth function. The reference compound HMPA had the longest measured  $T_1$  of 9.6 s, so the recycle delay was set at approximately five times this value (50 s) to allow for full relaxation to the thermal equilibrium distribution. For decoupling experiments,  $^1\text{H}$  inverse gated decoupling was applied via a WALTZ-16 sequence with 14.3 kHz bandwidth. For proper quantitation, experiments were performed in triplicate and  $^{31}\text{P}$  peaks were integrated and normalized against the peak area of the HMPA internal standard.

## 3. Results and discussion

### 3.1. Measurement of Catalyst $pK_a$ 's

The  $pK_a$  of the leaving group is dependent on the solvent and temperature, with literature values typically given for an aqueous solution at room temperature. Here, we used a matrix consisting of 50%  $\text{H}_2\text{O}$ , 37.5%  $\text{D}_2\text{O}$ , and 12.5%  $\text{CD}_3\text{CN}$  at 50 °C, necessitating a determination of the  $pK_a$ 's under these non-standard conditions. These experiments are described in [Supplementary Section S1](#). Briefly,  $^1\text{H}$  NMR chemical shifts were recorded at a variety of pH values and the  $pK_a$  values were obtained from a least-squares fitting procedure [26]. The results were as follows:  $\text{Zn}^{2+}$ -[12]aneN<sub>3</sub>,  $pK_a = 6.66 \pm 0.10$ ;  $\text{Zn}^{2+}$ -cyclen,  $pK_a = 7.75 \pm 0.13$ ;  $\text{Zn}^{2+}$ -cyclam,  $pK_a = 10.02 \pm 0.82$ ; AMPSO,  $pK_a = 8.06 \pm 0.11$ . A value of the  $pK_a$  for  $\text{Zn}^{2+}$ -[9]aneN<sub>3</sub> was not determined as its structure is still under debate.

### 3.2. NMR spectral assignment

$^{31}\text{P}$  NMR spectra were taken over several days to monitor the course of paraoxon degradation and subsequent generation of its byproducts.  $^{31}\text{P}$  chemical shifts for paraoxon, DEP, E4NPP, and HMPA were assigned as described in [Supplementary Section S2](#). The chemical shifts were as follows:  $\delta_{\text{Paraoxon}} = -6.73$  ppm,  $\delta_{\text{DEP}} = 0.60$  ppm,  $\delta_{\text{E4NPP}} = -5.11$  ppm,  $\delta_{\text{HMPA}} = 29.65$  ppm. A typical  $^{31}\text{P}$  NMR spectrum is shown in [Supplementary Fig. S2](#).

### 3.3. Degradation of paraoxon

[Fig. 1](#) shows the decrease in paraoxon  $^{31}\text{P}$  signal intensity associated with the degradation of paraoxon by the four catalysts under study. Background hydrolysis in AMPSO buffer alone is also given as a control. The data were taken at three to four time points each day over the course of a week and were normalized and fit using Origin 9.0 (OriginLab, Northampton, MA). The fit assumed

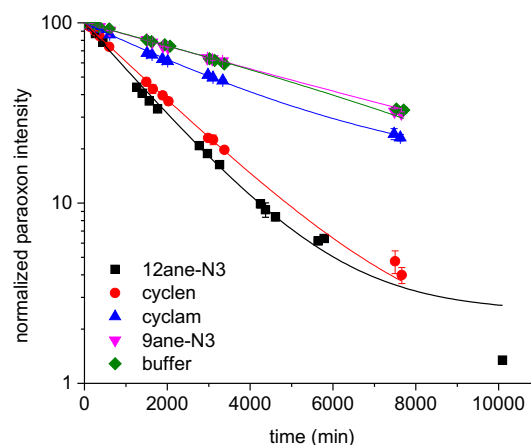


**Fig. 1.** Degradation of paraoxon at initial pH = 8.1 (0.1 M AMPSO) at 50 °C in the presence of each catalyst and a control consisting of buffer alone. Data were fit via nonlinear regression to a decaying exponential function with constant offset. “ $\text{Zn}^{2+}$ ” is omitted from all legends to increase readability.

first-order kinetics with a single exponential decay term plus offset,  $I = (100 - I_\infty) \exp(-t/\tau) + I_\infty$ . Here,  $I$  is the signal intensity at time  $t$ ,  $\tau$  is the reaction time constant ( $\tau = 1/k$ ), with  $k$  the overall pseudo-first order reaction rate constant, and  $I_\infty$  is the remaining intensity at long time points (offset). Further commentary on this point is given in [Section 3.9](#).

Paraoxon degradation in the presence of the  $\text{Zn}^{2+}$ -[12]aneN<sub>3</sub> catalyst was observed to occur rapidly compared to the other catalysts and the buffer. The cyclen-based complex displayed a slightly lower activity, while the cyclam-based complex displayed a small, but still enhanced activity. The  $\text{Zn}^{2+}$ -[9]aneN<sub>3</sub> complex displayed little hydrolytic activity, exhibiting only a slightly better kinetic rate than that due to buffer alone. The paraoxon data were described well by the single exponential decay rates given in [Table 1](#). Also given are the reaction time constants  $\tau$ .

It should be noted that the catalytic activities of these species are quite low, with only up to a five-fold enhancement over the hydrolysis rate in buffer alone for the best catalyst,  $\text{Zn}^{2+}$ -[12]aneN<sub>3</sub>. Such rates are hundreds of times slower than for catalyzed methanolysis of paraoxon using similar catalysts [27]. It should be kept in mind, however, that catalyzed methanolysis imposes an additional constraint on paraoxon decontamination – namely, the inclusion of methanol in the cleanup process. Real-world decontaminations are likely to be performed in aqueous environments, necessitating the use of large amounts of methanol for such catalysts. Moreover, any potential *in vivo* treatment applications must be conducted in an aqueous medium. Thus, an aqueous catalyst may be an advantage over one utilizing methanolysis, even if it has a significantly lower activity. Additional studies to improve the catalytic activity of these catalysts should be performed. For instance, covalent attachment to various members of the cyclodextrin family might allow the exploitation of an

**Table 1**

Pseudo-first order time constants, reaction rates, and half-lives for paraoxon degradation at initial pH = 8.1 (0.1 M AMPSO) at 50 °C in the presence of each catalyst and a control consisting of buffer alone. Data were fit to a decaying exponential function with constant offset.

Catalyst	$\tau$ (hr)	$k$ ( $\text{min}^{-1}$ , $\times 10^4$ )
$\text{Zn}^{2+}$ -[12]aneN <sub>3</sub>	$27.4 \pm 1.0$	$6.08 \pm 0.23$
$\text{Zn}^{2+}$ -cyclen	$33.0 \pm 0.8$	$5.05 \pm 0.12$
$\text{Zn}^{2+}$ -cyclam	$58.6 \pm 2.0$	$2.84 \pm 0.10$
$\text{Zn}^{2+}$ -[9]aneN <sub>3</sub>	$106 \pm 10$	$1.56 \pm 0.15$
Buffer (control)	$130 \pm 16$	$1.28 \pm 0.15$

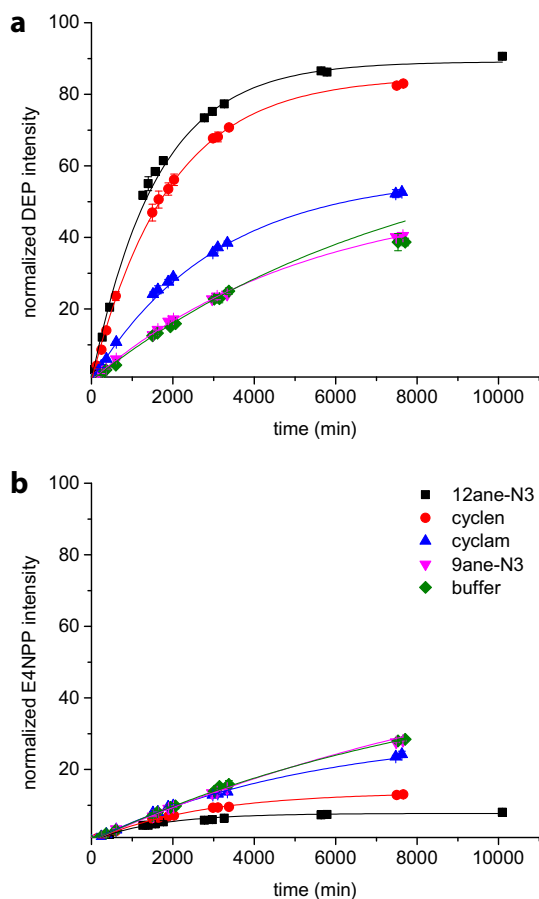


**Fig. 2.** (a) DEP generation and (b) E4NPP generation at initial pH = 8.1 (0.1 M AMPSO) at 50 °C in the presence of each catalyst and a control consisting of buffer alone. The legend given in (b) applies to the data in both (a and b). “Zn<sup>2+</sup>” is omitted from all legends to increase readability. The curves result from nonlinear least squares fits to single exponential growth functions but mainly serve to guide the eye.

additional hydrophobic interaction and substantially increase the catalytic rate.

### 3.4. Formation rates of DEP and E4NPP

Fig. 2a and b show the intensities for DEP and E4NPP formation, respectively, for all catalysts. Fig. 3 compares the paraoxon, DEP, and E4NPP <sup>31</sup>P intensities for the most effective catalyst, Zn<sup>2+</sup>-[12]aneN<sub>3</sub>. Prior to a more formal analysis, two conclusions can be made by inspection of these graphs: (1) regardless of the selectivity of the catalyzed hydrolysis for one byproduct over another, both DEP and E4NPP are generated in significant quantities; and (2) DEP formation is favored over E4NPP formation for catalysts with lower pK<sub>a</sub> values. Table 2 contains the reaction time constants for DEP formation extracted using a first order exponential growth model. Note that only for the Zn<sup>2+</sup>-[12]aneN<sub>3</sub> and Zn<sup>2+</sup>-cyclen catalysts is there statistical similarity in the values of  $\tau$  for paraoxon degradation (Table 1) and  $\tau_{DEP}$  for formation of DEP. This is due to the overall rate of paraoxon degradation,  $k$ , being a sum of the DEP and E4NPP reaction rates ( $k = k_{DEP} + k_{E4NPP}$ ). See Section 3.9 for a more detailed analysis.

### 3.5. Demonstration of reaction order

As demonstrated in Sections 3.3 and 3.4, the application of a single exponential decay term with offset seems to describe the data quite faithfully. For true first-order kinetics, a reactant is

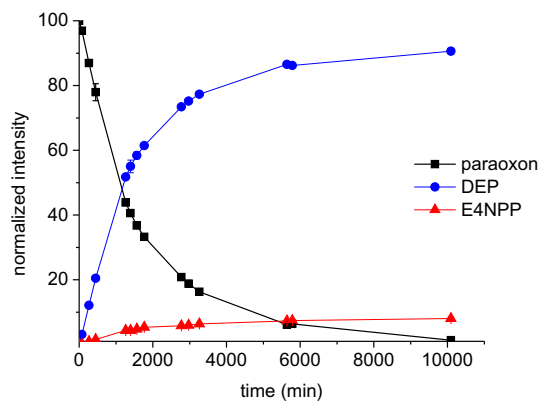


**Fig. 3.** Comparison of paraoxon, DEP, and E4NPP reaction profiles for 10 mol% (1.36 mM) Zn<sup>2+</sup>-[12]aneN<sub>3</sub> catalyst in pH = 8.1 (0.1 M AMPSO) at 50 °C. Curves are fits to single exponential functions but mainly serve to guide the eye.

**Table 2**

Pseudo-first order time constants,  $\tau_{DEP}$  ( $= k_{DEP}^{-1}$ ) for DEP formation at initial pH = 8.5 (0.1 M AMPSO) at 50 °C in the presence of each catalyst and a control consisting of buffer alone.

Catalyst	$\tau_{DEP}$ (h)
Zn <sup>2+</sup> -[12]aneN <sub>3</sub>	26.6 ± 0.7
Zn <sup>2+</sup> -cyclen	31.5 ± 0.8
Zn <sup>2+</sup> -cyclam	50.8 ± 1.4
Zn <sup>2+</sup> -[9]aneN <sub>3</sub>	87.5 ± 3.8
Buffer (control)	132 ± 47

simply converted to a product and the reaction is described by a single exponential decay. Catalytic reactions involving short-lived transition states are considered pseudo-first order, but are also well-described by single exponential functions. For each of these processes, the reaction rate is unaffected by initial substrate concentration (compared to, e.g., a Michaelis–Menten mechanism observed with dinuclear zinc complexes reported previously [28,29]). If paraoxon degradation by the zinc(II) catalysts in the present study behaves in a pseudo-first order manner, an increase in initial substrate concentration should not impact the overall reaction rate constant. Thus, we labored to determine the kinetic order by examining the effect of varying paraoxon concentration on the reaction rate time constant for the best catalyst, Zn<sup>2+</sup>-[12]aneN<sub>3</sub>. In these experiments, the catalyst concentration was kept constant at 1.36 mM Zn<sup>2+</sup>-[12]aneN<sub>3</sub>, or 10 mol% of the nominal 13.6 mM paraoxon initial concentration.

Fig. 4 shows how increased initial substrate concentration affects paraoxon degradation. At very short times, the reactions proceed similarly regardless of initial paraoxon concentration. It appears, however, that the reaction rate decreases with increasing initial paraoxon content for the long time data points (i.e. data collected after 1000 min). Table 3 contains reaction time constants for the 13.6 mM paraoxon concentration and increased concentrations of 20.4 mM, and 27.2 mM. These measurements represent 1.5× and 2.0× increases in the initial paraoxon concentration, respectively. Note that the reaction time constants are not strongly affected by varying the substrate concentration. Rather, it is the asymptotic behavior that is affected by increasing initial paraoxon content. That is, the offset  $I_{\infty}$  is observed to increase with paraoxon concentration. Additional analysis is provided in Section 3.9.

### 3.6. Product inhibition studies

It has been well documented that for a wide variety of metal-based catalysts, reaction products can be equally good ligands as

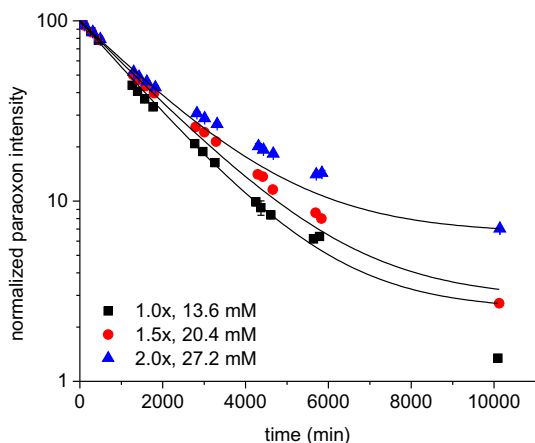


**Fig. 4.** Normalized paraoxon content as a function of initial paraoxon (substrate) concentration at initial pH = 8.1 (0.1 M AMPSO) at 50 °C for the catalyst  $\text{Zn}^{2+}$ -[12]ane- $\text{N}_3$  (1.36 mM). The curves represent single exponential decay terms with offsets.

**Table 3**

Pseudo-first order time constants for paraoxon degradation as a function of initial paraoxon concentration at initial pH = 8.1 (0.1 M AMPSO) at 50 °C for the catalyst  $\text{Zn}^{2+}$ -[12]ane- $\text{N}_3$  (1.36 mM).

[Paraoxon] (mM)	$\tau$ (h)
13.6	$27.4 \pm 1.0$
20.4	$30.4 \pm 0.2$
27.2	$31.2 \pm 0.4$

the desired ligand itself. This catalyst “poisoning” diminishes or eliminates catalytic ability and is known as product inhibition. For the zinc-azamacrocycles considered presently, it was not known if the phosphorus-containing byproducts DEP and E4NPP would behave in such a manner. Competition at the zinc center by these compounds would retard hydrolysis, precluding access to the active hydroxide.

To assess the impact of product inhibition on the catalysts studied presently, various amounts of 4-NP, a potential inhibitor formed during the generation of DEP, were added to an initial paraoxon concentration of 13.6 mM. The most effective catalyst,  $\text{Zn}^{2+}$ -[12]ane- $\text{N}_3$ , was present at a concentration of 1.36 mM (10 mol% relative to initial paraoxon concentration). Fig. 5 shows the impact on paraoxon degradation for 4-NP concentrations of 0.00 mM, 2.7 mM, and 5.4 mM (0, 20, and 40 mol%, respectively). The time constants for paraoxon degradation under these conditions are given in Table 4. At these concentrations of 4-NP, product inhibition does not seem to be a problem. A similar lack of product inhibition has been demonstrated for the catalytic hydrolysis of bis(4-nitrophenyl) phosphate by a dinuclear  $\text{Zn}^{2+}$  azamacrocyclic complex [30].

### 3.7. Effects of buffer concentration

To further investigate the impact of various reaction conditions on catalyst performance, the effects of buffer concentration were also considered. Fig. 6 compares results for the nominal 0.1 M AMPSO concentration to those obtained for 0.25 M and 0.5 M concentrations. The extracted reaction time constants, shown in Table 5, suggest that there is little effect of this concentration on the hydrolysis of paraoxon. Only at 0.5 M is there perhaps an increase in the overall rate of reaction, but that difference is slight.

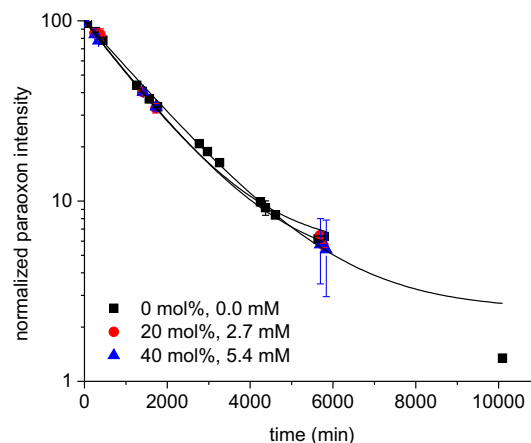


**Fig. 5.** Effect of product inhibition via 4-nitrophenol (4-NP) on paraoxon degradation at initial pH = 8.1 (0.1 M AMPSO) at 50 °C for the catalyst  $\text{Zn}^{2+}$ -[12]ane- $\text{N}_3$  (1.36 mM). Concentrations of 4-NP are relative to an initial paraoxon concentration of 13.6 mM. Curves are the result of fits to decaying exponential functions with constant offsets.

**Table 4**

Pseudo-first order time constants for paraoxon degradation as a function of 4-nitrophenol (4-NP) concentration at initial pH = 8.1 (0.1 M AMPSO) at 50 °C for the catalyst  $\text{Zn}^{2+}$ -[12]ane- $\text{N}_3$  (1.36 mM).

[4-NP] (mM)	$\tau$ (h)
0.00	$27.4 \pm 1.0$
2.72	$24.0 \pm 1.7$
5.44	$23.3 \pm 2.0$

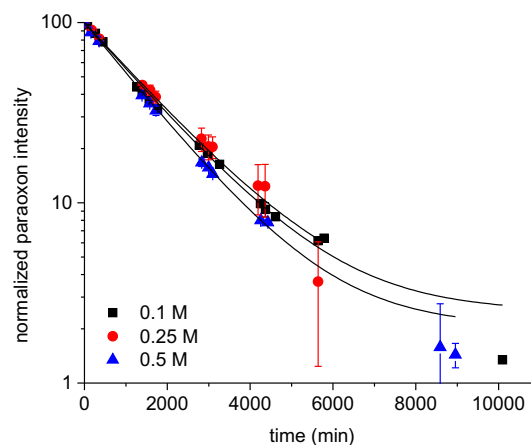


**Fig. 6.** Effect of buffer concentration on paraoxon content at initial pH = 8.1 at 50 °C for the catalyst  $\text{Zn}^{2+}$ -[12]ane- $\text{N}_3$  (1.36 mM) and an initial paraoxon concentration of 13.6 mM. Curves are the result of fits to decaying exponential functions with constant offsets.

**Table 5**

Pseudo-first order time constants for paraoxon degradation as a function of buffer concentration at initial pH = 8.1 at 50 °C for the catalyst  $\text{Zn}^{2+}$ -[12]ane- $\text{N}_3$  (1.36 mM) and an initial paraoxon concentration of 13.6 mM.

[Buffer] (M)	$\tau$ (h)
0.10	$27.4 \pm 1.0$
0.25	$28.4 \pm 0.6$
0.50	$25.4 \pm 0.3$

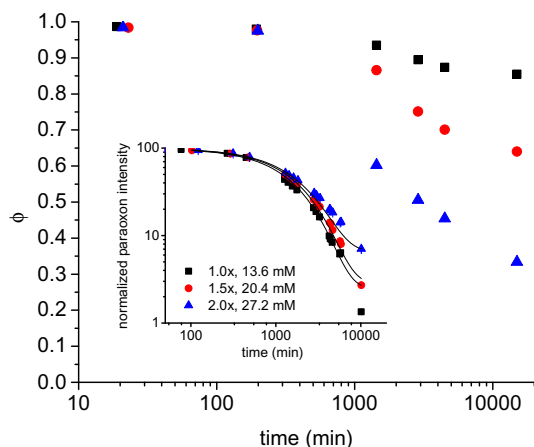


**Fig. 7.** Effect of initial paraoxon concentration on active  $\text{Zn}^{2+}$ -[12]ane $\text{N}_3$  fraction,  $\phi$ , for 0.1 M AMPSO buffered solutions at 50 °C and 1.36 mM  $\text{Zn}^{2+}$ -[12]ane $\text{N}_3$ . Initial paraoxon concentrations are given as multiples of the nominal value of 13.6 mM. (inset) Semi-log plot of paraoxon concentration for comparison to pH data (data identical to that presented in Fig. 5).

### 3.8. Acid generation effects

Despite the presence of buffer, significant acid generation due to paraoxon degradation could result in a pH decrease, thereby decreasing the fraction of active catalyst. Because the effective reaction rate of a pseudo-first order catalytic reaction is dependent on catalyst concentration, this decrease in active catalyst would result in a time-dependent rate constant  $k = k(t)$  over the course of the observed reaction and a marked deviation from a simple exponential decay. While this single exponential term seemed to describe most of the data reported currently, the data considered have shown a slight departure from simple exponential decay at long time data points. In non-linear least squares fits to these data, this manifests as a relatively small change in overall reaction rate but a dramatic difference in the asymptotic behavior of the paraoxon degradation profile.

Because the products DEP and E4NPP are both acids, the pH was monitored as a function of time for the variable substrate concentration samples. These time-dependent pH values were then converted to active  $\text{Zn}^{2+}$ -[12]ane $\text{N}_3$  fractions,  $\phi(t)$  via

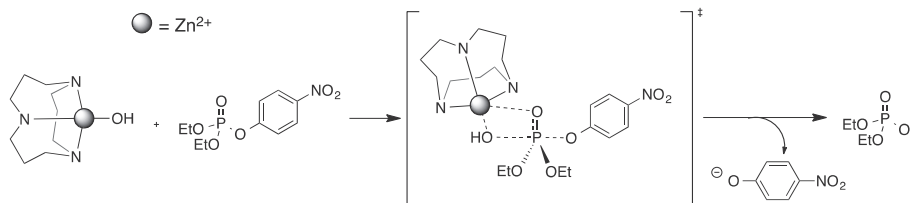
$$\phi(t) = \frac{10^{(\text{pH}(t) - \text{pK}_a)}}{1 + 10^{(\text{pH}(t) - \text{pK}_a)}} \quad (1)$$

where  $\text{pK}_a = 6.66$  for this catalyst. Results are given in Fig. 7.

The behavior of pH and paraoxon concentration are similar amongst the three initial substrate conditions at short time data points. For pH data beyond ca. 1000 min (0.69 days), however, there are dramatic differences amongst the pH of the samples, with higher initial paraoxon concentrations yielding increasingly more acidic samples. The same divergence can be seen for the time-dependent paraoxon concentration. The decrease in pH results in asymptotically lower values of  $\phi$ . For example, at the last time point taken (15000 min = 10.4 days) the pH of the 1.0 $\times$ , 1.5 $\times$ , and 2.0 $\times$  samples were 7.43, 6.91, and 6.36, respectively. At these pH values,  $\phi$  are calculated to be 85%, 64%, and 33%, respectively.

Though buffers are used to regulate solution pH, they are only generally effective for sample pH values within approximately one unit of the buffer  $\text{pK}_a$ . For AMPSO in our mixture of 4:3:1 mixture of  $\text{H}_2\text{O}:\text{D}_2\text{O}:\text{CD}_3\text{CN}$  at 50 °C, this pH range spans from approximately 7.50 to 8.70. It is not surprising, then, that there exists such a precipitous decline in pH for all three samples at long time points where the pH drops below approximately 7.5, the lower limit of AMPSO's ability to buffer. As the reaction progresses beyond this lower bound, the AMPSO buffering capability decreases and the growing acid content strongly impacts the sample pH. Note that this lower pH threshold of 7.5 is surpassed even for the nominal paraoxon concentration of 1.38 mM. This implies that for every experiment considered herein, the sample pH was lower than 7.5 at some point, and there was a significant decline in  $\phi$ . This fact urged the use of an offset term to approximate the effect of a decline in catalyst activity. Note that for a buffer with a lower  $\text{pK}_a$  (e.g., HEPPS;  $\text{pK}_a = 8.1$  at 20 °C) an offset may not have to be considered because the pH would remain within the buffer's working range.

In summary, changes in pH due to increased acid generation and AMPSO's failure to buffer acidic samples beyond a pH of 7.5 ultimately explain why there remains more paraoxon for larger initial substrate concentrations. Note, however, that the rate of reaction using the  $\text{Zn}^{2+}$ -[12]ane $\text{N}_3$  catalyst is always higher than that of the control, as some fraction of catalyst is always in its active hydroxide state. Any additional substrate simply generates more acidic hydrolysis products over time, thereby decreasing the sample pH and inactivating a larger percentage of the  $\text{Zn}^{2+}$ -



**Scheme 3.** Proposed mechanism for the degradation of paraoxon to DEP via a weakly associated transition state. Structure derived from Refs. [31,32].

**Table 6**  
Pseudo-first order reaction rate constants and selectivities for DEP and E4NPP formation from nonlinear least squares analysis of NMR kinetic data using Eqs. (1–3). All experiments were performed at initial pH = 8.1 (0.1 M AMPSO) at 50 °C for catalyst concentrations of 10 mol% relative to an initial paraoxon concentration of 13.6 mM.

Catalyst	$k_{\text{DEP}}$ ( $\text{min}^{-1}$ , $\times 10^4$ )	$k_{\text{E4NPP}}$ ( $\text{min}^{-1}$ , $\times 10^4$ )	S	$k$ ( $\text{min}^{-1}$ , $\times 10^4$ )
$\text{Zn}^{2+}$ -[12]ane $\text{N}_3$	$5.56 \pm 0.47$	$0.506 \pm 0.098$	$11.0 \pm 2.3$	$6.06 \pm 0.48$
$\text{Zn}^{2+}$ -cyclen	$4.32 \pm 0.15$	$0.630 \pm 0.058$	$6.9 \pm 0.7$	$4.95 \pm 0.16$
$\text{Zn}^{2+}$ -cyclam	$1.59 \pm 0.10$	$0.652 \pm 0.067$	$2.4 \pm 0.3$	$2.25 \pm 0.18$
$\text{Zn}^{2+}$ -[9]ane $\text{N}_3$	$0.919 \pm 0.046$	$0.591 \pm 0.052$	$1.6 \pm 0.2$	$1.51 \pm 0.07$
Buffer (control)	$0.878 \pm 0.077$	$0.602 \pm 0.086$	$1.5 \pm 0.2$	$1.48 \pm 1.12$

**Table 7**

Second-order reaction rate constants  $k'$  for  $\text{Zn}^{2+}$ -[12]aneN<sub>3</sub>,  $\text{Zn}^{2+}$ -cyclen, and  $\text{Zn}^{2+}$ -cyclam. All values are calculated from the pseudo-first-order rate constants  $k$  in Table 6 and active catalyst concentrations determined using the Henderson–Hasselbalch equation and a nominal catalyst concentration of 1.36 mM.

Catalyst	$k'$ ( $\text{min}^{-1} \text{mM}^{-1}$ )
$\text{Zn}^{2+}$ -[12]aneN <sub>3</sub>	$34.9 \pm 3.6$
$\text{Zn}^{2+}$ -cyclen	$29.8 \pm 2.0$
$\text{Zn}^{2+}$ -cyclam	$179 \pm 329$

[12]aneN<sub>3</sub> catalyst. Reaction rates are relatively unaffected, however, because the pH changes are negligible at early times where the magnitudes of  $k$  are more reliably determined.

These considerations also have an impact on the data described in Fig. 6. There appears to be very little effect of buffer concentration on paraoxon degradation even for the highest buffer content of 0.5 M. The elevated temperature at which the experiments were conducted lowered the pH of the samples. Acids generated as a result of hydrolysis would further decrease this pH over time, creating sample conditions for which AMPPO no longer serves as an effective buffer. Therefore, decreasing pH negates the effects of increased buffer concentration on the observed rate of hydrolysis for these samples.

### 3.9. Hydrolysis product distribution

Phosphotriester hydrolysis under basic conditions proceeds via nucleophilic attack of the phosphorus, which forms some degree of associative intermediate with the more acidic leaving group oriented apical to the nucleophile (Scheme 3) [31–33]. In the case of paraoxon, the 4-nitrophenoxy moiety (with a low  $\text{pK}_a$  of 7.0 compared to 16.0 for ethanol) [34] should occupy the apical position and be preferentially hydrolyzed from the molecule, leaving DEP as the dominant phosphorus-containing product.

As discussed in Section 3.2, however, there are samples where E4NPP is generated in significant quantities. For pseudo-first order kinetics, the ratio of the products (or selectivity,  $S = [\text{DEP}]/[\text{E4NPP}]$ ) is expected to be time-invariant; however, the data in this study yield a range of  $S$  values due to fluctuations in experimental conditions, poor NMR signal-to-noise, and measurement error. To extract additional reaction rate information and more accurately calculate product selectivity, simultaneous nonlinear regression was performed for all phosphorus-containing species for each catalyst. Maintaining that the hydrolysis is pseudo-first-order, the one-reactant, two-product reaction scheme can be analyzed straightforwardly. Note, however, that for the present purposes the effect of pH (i.e. time-dependent reaction rates, as discussed in Section 3.7) has been ignored. The time-dependent normalized concentrations  $[P](t)$ ,  $[\text{DEP}](t)$ , and  $[\text{E4NPP}](t)$  of paraoxon, DEP, and E4NPP, respectively, are described by a series of coupled, linear differential equations whose solutions are:

$$\frac{[P](t)}{[P_0]} = e^{[-(k_{\text{DEP}} - k_{\text{E4NPP}})t]} \quad (2)$$

$$\frac{[\text{DEP}](t)}{[P_0]} = \frac{k_{\text{DEP}}}{k_{\text{DEP}} + k_{\text{E4NPP}}} (1 - e^{[-(k_{\text{DEP}} - k_{\text{E4NPP}})t]}) \quad (3)$$

$$\frac{[\text{E4NPP}](t)}{[P_0]} = \frac{k_{\text{E4NPP}}}{k_{\text{DEP}} + k_{\text{E4NPP}}} (1 - e^{[-(k_{\text{DEP}} - k_{\text{E4NPP}})t]}) \quad (4)$$

where  $k_{\text{DEP}}$  and  $k_{\text{E4NPP}}$  are the formation rates of DEP and E4NPP, respectively, and  $[P_0]$  is the initial concentration of paraoxon. The exponential terms in Eqs. (2) and (3) go to zero at long times, leaving the long-time selectivity  $S = k_{\text{DEP}}/k_{\text{E4NPP}}$ . Eqs. (1–3) were fit

simultaneously in Mathematica 9 (Wolfram Research, Champaign, IL) using a nonlinear least squares fitting approach. The resultant values of  $k_{\text{DEP}}$ ,  $k_{\text{E4NPP}}$ , and  $S$  are given in Table 6. Graphs of fit results are given in Supplementary Section S3 and Supplementary Figs. S3–S7, and demonstrate that, while the effect of decreased pH on  $\phi$  and reaction rates is ignored, the quality of the fits is excellent.

This more detailed analysis yields values for paraoxon degradation that are strikingly similar to those calculated from the more simplistic data analysis in Section 3.2 and summarized in Table 1. Recall that estimates for  $\tau_{\text{DEP}}$  (Table 2) only compared well with  $\tau$  for paraoxon degradation for low  $\text{pK}_a$  catalysts which produced DEP as the overwhelming product. A more thorough analysis using Eqs. (2–4) reveals why values of  $\tau_{\text{DEP}}$  diverge from  $\tau$  when considering the  $\text{Zn}^{2+}$ -cyclam,  $\text{Zn}^{2+}$ -[9]aneN<sub>3</sub>, and control samples: for less effective catalysts with smaller initial  $\phi$ , E4NPP formation becomes more important. However, the rate of formation of E4NPP is largely invariant among samples, having an average value of  $0.596 \pm 0.056 \times 10^{-4} \text{ min}^{-1}$ . This strongly suggests that E4NPP generation is due to background hydrolysis only and that product selectivity depends primarily on catalyst activity. That is, all catalysts overwhelmingly prefer the generation of DEP.

As discussed above, the fraction of catalyst in its active state is dictated largely by the difference in  $\text{pK}_a$  relative to the pH of the medium. The Henderson–Hasselbalch equation dictates that a larger difference between sample pH and catalyst  $\text{pK}_a$  produces a higher fraction of catalyst in the active hydroxide state. For  $\text{Zn}^{2+}$ -[12]aneN<sub>3</sub>,  $\text{Zn}^{2+}$ -cyclen, and  $\text{Zn}^{2+}$ -cyclam, the pseudo-first order reaction rates correlate well with the active catalyst fraction (linear fit,  $R^2 = 0.986$ ). We can further quantify this by examining second-order rate constants  $k'$ , calculated according to  $k' = k_{\text{cat}}/[\text{cat}]$  where  $[\text{cat}]$  is the active catalyst concentration. Second-order rate constants accounting for the fraction of active catalyst  $\phi$  are shown in Table 7. We do not provide data for  $\text{Zn}^{2+}$ -[9]aneN<sub>3</sub>, as its structure is still under debate, or for the buffer. In addition, the uncertainty in the second-order rate constant for  $\text{Zn}^{2+}$ -cyclam is quite large. This is a result of the very small value and high uncertainty in  $\phi$  for this species; the low value results from the catalyst having a  $\text{pK}_a$  of 10.02, much larger than the starting pH of 8.1, while the high uncertainty results from the presence of multiple catalyst conformers. Given this large uncertainty, we do not place much weight on the apparently high but statistically insignificant second-order rate constant for  $\text{Zn}^{2+}$ -cyclam presented in Table 7.

Zinc-azamacrocyclic catalyst preference for DEP generation warrants additional discussion. Hydrolysis of phosphotriesters has been discussed in regards to both electrostatic and steric effects on the reaction free energy barrier [35,36]. For ester groups of like  $\text{pK}_a$ , it has been shown that larger side groups increase this barrier, making reaction rates subsequently smaller. Despite the size of the 4-NP group of paraoxon, its low  $\text{pK}_a$  makes it the overwhelmingly likely leaving group. For the buffer control, however, there is very little favorability for DEP formation at 50 °C. At this elevated temperature, thermodynamic determinants like  $\text{pK}_a$  no longer matter, and roughly equimolar amounts of DEP and E4NPP are observed to form ( $S = 1.5 \pm 0.2$ ). In none of the samples was generation of E4NPP dominant. Moreover, DEP formation far outweighs E4NPP formation for additional experiments performed at reduced temperatures, a regime in which relative  $\text{pK}_a$  values strongly dictate product formation. For these data, see Supplementary Section S4, Supplementary Figs. S8–S9, and Supplementary Table S1.

This is consistent with the observation of preferential cleavage of 4-NP from diphenyl (4-nitrophenol) phosphate (phenol  $\text{pK}_a = 9.99$  relative to 4-NP  $\text{pK}_a = 7.15$ ) for both catalytic and alkaline hydrolysis [31]. In that work, however, selectivity

decreased when using  $\text{Zn}^{2+}$ -based catalysts, generating more phenyl (4-nitrophenol) phosphate than under alkaline conditions. The current data reveal the opposite trend: employing catalysts with decreased  $\text{pK}_a$  dramatically increases the selectivity towards DEP formation.

### 3.10. Catalytic mechanism

To explain catalyst preference for DEP, it is important to consider both the structure of the active catalyst and that of the transition state. As with typical  $\text{S}_{\text{N}}2$  and  $\text{S}_{\text{N}}2$ -like reactions, nucleophilic attack by the hydroxide anion in purely alkaline conditions occurs opposite the leaving group. The resultant rate-determining intermediate [35,36] converts the otherwise tetrahedral phosphate arrangement into a trigonal bipyramidal-like, weakly associative transition state with the nucleophilic hydroxide ion and leaving group at apical positions [31]. In the case of this basic hydrolysis, hydroxide ions have relatively free access to attack the phosphorus atom from a variety of trajectories.

For the current catalysts, the hydroxide is coordinated to the metallo-azamacrocyclic ligand, and the size of this complex is expected to increase the free energy barrier for reaction. For paraoxon hydrolysis, either an ethoxy or 4-nitrophenoxy group assumes the apical position in the transition state. Given that the 4-nitrophenoxy group is highly conjugated and rigid, it is more likely that it would adopt a position opposite the catalyst's hydroxide anion and away from the relatively bulky hydroxide–zinc–ligand complex. It is also possible that this conformation is more likely from a thermodynamic standpoint, resulting in a more stable transition state than if the 4-nitrophenoxy group were to adopt an equatorial position more proximate to the catalyst.

The effects of sterics on catalytic activity of these and similar complexes have received a considerable amount of discussion [36]. While a large variety of nitrogen-containing molecules have been studied for their activity as ligands for organometallic catalysts, little if any fundamental physical chemical reasoning has been offered to explain if and how bulky ligands and their substituents affect observed byproduct formation and, in particular, byproduct selectivity. This aspect deserves further consideration, particularly since discrepancies between these and other data remain. Computational simulation can provide considerable insight into the role that steric effects play with regard to catalytic activity and selectivity. Research is currently underway to investigate these subtleties.

## 4. Conclusions

A series of Zn(II) azamacrocyclic catalysts were synthesized and studied for their efficacy towards the hydrolysis of paraoxon, an organophosphate pesticide, in aqueous media. The main physical property dictating catalyst hydrolytic ability is its  $\text{pK}_a$  relative to the pH of the medium, and the most active catalyst investigated was the catalyst with the lowest  $\text{pK}_a$ , the 1,5,9-triazacyclododecane-Zn(II) complex,  $\text{Zn}^{2+}$ -[12]aneN<sub>3</sub> ( $\text{pK}_a = 7.3$ ). The effects of sample pH, buffer content, and inhibition by the reaction byproduct 4-nitrophenol were also investigated. It was found that buffer content and product inhibition effects were minimal. Sample pH and, more specifically, pH changes due to acid generation, however, were shown to have a large effect on paraoxon degradation. These effects were particularly acute for samples with increased initial paraoxon concentrations, as the additional acid generated rapidly lowered the pH beyond the working pH range of the AMPSO buffer. This phenomenon resulted in a precipitous decline in paraoxon degradation due to catalyst inactivation by the increasingly acidic sample conditions. Modifying the choice of

buffering agent to accommodate this change in sample acidity is recommended and work is ongoing to investigate the effects of other organic buffers with lower  $\text{pK}_a$  values. Other Zn(II) catalysts are also currently being synthesized and investigated with the goal of maximizing hydrolytic efficiency.

## Acknowledgements

This work was performed under the auspices of the U.S. Department of Energy by Lawrence Livermore National Laboratory under Contract DE-AC52-07NA27344 and support from Lawrence Livermore National Laboratory (14-ERD-048). This document (LLNL-JRNL-663756) was prepared as an account of work sponsored by an agency of the United States government. Neither the United States government nor Lawrence Livermore National Security, LLC, nor any of their employees makes any warranty, expressed or implied, or assumes any legal liability or responsibility for the accuracy, completeness, or usefulness of any information, apparatus, product, or process disclosed, or represents that its use would not infringe privately owned rights. Reference herein to any specific commercial product, process, or service by trade name, trademark, manufacturer, or otherwise does not necessarily constitute or imply its endorsement, recommendation, or favoring by the United States government or Lawrence Livermore National Security, LLC. The views and opinions of authors expressed herein do not necessarily state or reflect those of the United States government or Lawrence Livermore National Security, LLC, and shall not be used for advertising or product endorsement purposes.

## Appendix A. Supplementary material

Supplementary data associated with this article can be found, in the online version, at <http://dx.doi.org/10.1016/j.ica.2015.07.035>.

## References

- [1] C.E. Furlong, W.F. Li, R.J. Richter, D.M. Shih, A. Lulis, E. Alleve, L.G. Costa, *Neurotoxicology* 21 (2000) 91.
- [2] T.B. Cole, K. Jansen, S. Park, W.F. Li, C.E. Furlong, L.G. Costa, *Adv. Exp. Med. Biol.* 660 (2001) 47.
- [3] P.G. Kopf, M.K. Walker, *Environ. Carcinog. Ecotoxicol. Rev.* 27 (2009) 276.
- [4] D. Mackay, J.P. Giesy, K.R. Solomon, *Rev. Environ. Contam. Toxicol.* 231 (2014) 35.
- [5] L.N. Konda, Z. Pasztor, *J. Agric. Food Chem.* 49 (2001) 3859.
- [6] E. Kimura, H. Hashimoto, T. Koike, *J. Am. Chem. Soc.* 118 (1996) 10963.
- [7] T. Koike, S. Kajitani, I. Nakamura, E. Kimura, M. Shiro, *J. Am. Chem. Soc.* 117 (1995) 1210.
- [8] P.R. Norman, *Inorg. Chim. Acta* 130 (1987) 1.
- [9] T. Koike, E. Kimura, *J. Am. Chem. Soc.* 113 (1991) 8935.
- [10] S.A. Melnychuk, A.A. Neverov, R.S. Brown, *Angew. Chem., Int. Ed. Engl.* 45 (2006) 1767.
- [11] M. Kruppa, D. Frank, H. Leffler-Schuster, B. König, *Inorg. Chim. Acta* 359 (2006) 1159.
- [12] D. Kong, X. Huang, Y. Xie, *Inorg. Chim. Acta* 340 (2002) 133.
- [13] C.M. Sarther, E.L. Blinn, *Inorg. Chem.* 15 (1976) 3083.
- [14] G. Ferraudi, J.C. Canales, B. Kharisov, J. Costamagna, J.G. Zagal, G. Cardenas-Jirón, M. Paez, *J. Coord. Chem.* 58 (2005) 89.
- [15] R.L. Gustafson, A.E. Martell, *J. Am. Chem. Soc.* 84 (1962) 2309.
- [16] J. Chin, X. Zou, *J. Am. Chem. Soc.* 110 (1988) 223.
- [17] L. Koziol, C.A. Valdez, S.E. Baker, E.Y. Lau, W.C. Floyd III, S.E. Wong, J.H. Satcher Jr., F.C. Lightstone, R.D. Aines, *Inorg. Chem.* 51 (2012) 6803.
- [18] X. Zhang, R. van Eldik, T. Koike, E. Kimura, *Inorg. Chem.* 32 (1993) 5749.
- [19] X. Zhang, R. van Eldik, *Inorg. Chem.* 34 (1995) 5606.
- [20] E. Kimura, T. Shiota, T. Koike, M. Shiro, M. Kodama, *J. Am. Chem. Soc.* 112 (1990) 5805.
- [21] L.L. Kiefer, J.F. Krebs, S.A. Paterno, C.A. Fierke, *Biochemistry* 32 (1993) 9896.
- [22] Y.-C. Yang, L.L. Szafraniec, W.T. Beaudry, D.K. Rohrbaugh, *J. Am. Chem. Soc.* 112 (1990) 6621.
- [23] Y.-C. Yang, J.A. Baker, J.R. Ward, *Chem. Rev.* 92 (1992) 1729.
- [24] Y.-C. Yang, L.L. Szafraniec, W.T. Beaudry, C.A. Bunton, *J. Org. Chem.* 58 (1993) 6964.
- [25] Y.-C. Yang, *Acc. Chem. Res.* 32 (1999) 109.
- [26] J. Bezencon, M.B. Wittwer, B. Cutting, M. Smiesko, B. Wagner, M. Kansy, B. Ernst, *J. Pharm. Biomed. Anal.* 93 (2014) 147.
- [27] T. Liu, A.A. Neverov, J.S.W. Tsang, R.S. Brown, *Org. Biomol. Chem.* 3 (2005) 1525.

- [28] L.J. Zompa, T.N. Margulis, *Inorg. Chim. Acta* 28 (1979) L157.
- [29] J.S. Alper, L.J. Zompa, *J. Inorg. Nucl. Chem.* 42 (1980) 1693.
- [30] M. Subat, K. Woinaroschy, C. Gerstl, B. Sarkar, W. Kaim, B. König, *Inorg. Chem.* 47 (2008) 4661.
- [31] S.H. Gellman, R. Petter, R. Breslow, *J. Am. Chem. Soc.* 108 (1986) 2388.
- [32] S.R. Caldwell, F.M. Raushel, P.M. Weiss, W.W. Cleland, *Biochemistry* 30 (1991) 7444.
- [33] M.A. Anderson, H. Shim, F.M. Raushel, W.W. Cleland, *J. Am. Chem. Soc.* 123 (2001) 9246.
- [34] W.P. Jencks, J. Regenstein, *Ionization Constants of Acids and Bases. Handbook of Biochemistry and Molecular Biology*, CRC Press, Cleveland, OH, 1976, p315.
- [35] F. Zheng, C.-G. Zhan, R.L. Ornstein, *J. Chem. Soc. Perkin Trans. 2* (12) (2001) 2355.
- [36] Y. Xiong, C.-G. Zhan, *J. Org. Chem.* 69 (2004) 8451.